Measurement Report: New particle formation characteristics at an urban and a mountain station in Northern China by Ying Zhou et al.

In this file, the referee comments are in black, our item-by-item replies are in blue, and the corresponding modifications in the manuscript are in red.

Answers to reviewer # 2

This work reported simultaneous measurements of new particle formation at an urban and mountain station in Northern China. The manuscript fits well to the scope of ACP, however, I do not think it represented new results or findings. The paper is worth to be published, but not in its current form. Thus I recommend it to be resubmitted if more analysis or dataset could be included.

Lots of paper about NPF in North China Plain have been published. I would suggest the authors demonstrate the new findings compared to the previous studies. As a measurement report, it only present one month data, I think this is enough. The conclusions did not show anything new.

The authors pointed out that NPF events at urban areas could have a bigger influence on global/regional climate and air pollution than those at clean areas. This should be considered in regional-scale aerosol models when estimating the budget of aerosol and CCN loadings. I agree with this, but how could we deal with it in the model. Maybe some exemplary cases and detailed discussions are more convincing.

As per suggestion of the referee, we extend our data set at urban Beijing (UB) to include two full summers (from June 1 to August 31) in 2018 and 2019. With the extended data, we updated our discussion on favorable and limiting factors on NPF event occurrence at the urban Beijing station. We also estimated the size of the area within which regional NPF events occurred during our observations. This estimation could possibly explain the phenomena that most ending diameters of NPF events during our observation were limited below 70 nm. Our results highlight the importance of anthropogenic emissions for NPF occurrence and subsequent growth in summer Beijing. Unfortunately, we were not able to

include more data from the background mountain station (MT), since no long-term measurements were maintained. As the results of this study, show also the contribution of the MT in forming particles, our study highlights the importance of establishing and maintaining long term measurement not only in urban location but also in rural ones.

Addition to the methods' section:

2.4 Estimating the spatial extent of NPF

The observation of regional new particle formation events, where the growth of newly formed particles can be followed for several hours, is a result of NPF taking place over a large spatial area. This is because as time progresses, the particles observed at a measurement site must have originated from further and further away due to non-zero wind conditions. Following the progression of the observed NPF event and using air mass back trajectories, we can estimate where the particles observed at different stages of the NPF event were initially formed by calculating the air mass locations at the onset time of the NPF event (assuming that NPF occurs simultaneously over the larger area). Typically, the mode related to the NPF event disappears from the observations after some time. This is an indication of the currently observed air mass arriving from an area where NPF was no longer taking place due to unfavorable local conditions. If the shift in the air mass origin towards unfavorable conditions occurs gradually over time, the mode related to the NPF event can enter a stage of growth stagnation (or even decrease in size) before disappearing completely (Kivekäs et al., 2016). This is because the increasing transport time between NPF onset and observation of the particles at the measurement site provides less and less additional 'material' for aerosol growth towards the more unfavorable conditions. Calculating the locations where NPF is assumed to have taken place for longer data sets including several regional NPF events can give an estimation of the typical spatial extent of NPF around the measurement location. It should be noted that even in relatively clear cases, the subjective determination of NPF event onset and end times can easily lead to uncertainties of few tens of kilometers in the estimations. In locations with strong primary pollution sources, such as urban Beijing, objective determination of said times becomes even more difficult. More details and discussion related to the method and its uncertainties can be found in Kristensson et al.

(2014).

Addition to Results section:

3.1.1 Favorable air mass origin for NPF events at individual locations

In Fig.R1, we show frequencies of air masses arriving at UB station from different directions during our observation in summer 2018 and 2019. The most frequent air masses arriving at UB station belonged to the South group. During our observation in the two summers, out of 155 days were 52 days belonging to the South group and 39, 32, 9 and 23 days in air masses belong to North, East, West and Local groups, respectively. NPF event frequency with respect to air masses is also shown in Fig. R1. It is noticeable that air mass origin influenced the occurrence of NPF events at UB site as the majority of NPF events occurred when the air masses were coming from the north. During our observation in summer 2018 and 2019, 34 (out of 55) NPF events occurred in air masses from the North group and 9, 2, 2 and 6 NPF events in the South, East, West and Local groups, respectively (Fig.R1a). One prominent feature of these air masses is their difference in CS. As shown in Fig. R1b, the CS of the air masses classified as the North group (with median values of 0.01 s^{-1} at UB station) is substantially lower than that in other air mass classes (CS = 0.03, 0.025, 0.017, 0.03 s^{-1}, for south, east, west and local, respectively), which might explain the high NPF event frequency associated with this air mass class. During the observation from June 14 to July 14 in summer 2019, the most frequent air masses arriving at both sites belonged to the North group as shown in Table 1. Out of 25 days, there were 8 and 9 days belonging to the North group, at UB and MT sites, respectively. The highest frequency of NPF events also occurred when the air masses were coming from the north. The high NPF events frequency during our observation form June 14 to July 14 could also be attributed to the frequent air masses arriving at both sites from north to Beijing.

3.1.2 The role of condensation sink in NPF event occurrence

Figure R2a shows the difference in CS between NPF event and non-event days during our observation in summer 2018 and 2019（two whole summers）at UB site and short-term parallel observations at both sites. The ‘NPF1’ and ‘non-event1’ referred to NPF and non-event days during the two whole summers, respectively, while ‘NPF2’ and ‘non-event2’ referred to NPF and non-event days during the short-term parallel observation period from

June 14 to July 14, 2019 at both sites, respectively. The longer-term periods are used for confirming the representativeness of the short-term overlapping period for the whole summer. As shown in the figure, the median CS on NPF1 or NPF2 days is equivalent for UB station (CS_{NPF1} = 0.010s^{-1}; CS_{NPF2}= 0.009s^{-1}) and less than a factor of 1.2 different between non-event1 and non-event2 in UB station ($CS_{nonevent1}$ = 0.023s^{-1}; $CS_{nonevent2}$= 0.020s^{-1}), which confirms the representativeness of our short-term measurement period to the overall urban Beijing summer.

Our results in figure R2a show that on NPF event days, the median CS was ~ 0.01 s^{-1} during the first 2 hours of the NPF events, at both stations. On common NPF event days, the median CS was 0.009 s^{-1} at UB station and ~0.01s^{-1} at MT station, respectively. In comparison, on non-event days, during roughly the same time period (9:00–11:00 LT), the CS was substantially higher, with median values of 0.02 s^{-1} and 0.014 s^{-1}, at UB and MT stations, respectively. Figure R2b presents the median CS during the first 2 hours of NPF events on common NPF event days measured at both stations, and shows the high correlation between the two.

Figure R2c shows the NPF event frequency as a function of CS during our observation at UB site in summer 2018 and 2019 and how the NPF event frequency decreased with increasing CS. When CS was smaller than 0.01 s^{-1}, all days were classified as NPF event days, and when CS was larger than 0.035 s^{-1}, no day was classified as NPF event day. This shows the major role of background particles in controlling the occurrence or inhibition of NPF events as shown in several previous studies in China and internationally (Deng et al., 2020a; Cai et al., 2017; Kulmala et al., 2017). While we cannot present a similar figure from the MT station, the same conclusion applies where CS does play a role in inhibiting NPF observation owing to the difference in the CS values observed between NPF and nonevents at MT in figure R2a. Yet, since the overall preexisting particle concentration at the MT is rather on the low end, the role of CS might not be as vital at the MT station as for the UB station.

3.1.4 Role of sulfuric acid concentrations in NPF event occurrence

In Fig. R3a, we show the concentration of sulfuric acid as a function of CS during summer 2018 and 2019 at UB site. As shown in Fig. R3b, the median sulfuric acid (H_2SO_4) concentrations at UB station were 8.1×10^6 cm^{-3} and 4.5 ×10^6 cm^{-3} on NPF event days and

non-event days, respectively, during observation from June 14 to July 14 in 2019 and 7.9×10^6 cm^{-3} and 3.4×10^6 cm^{-3} on NPF event days and non-event days, respectively, during the observation in summer 2018 and 2019. This suggests that H_2SO_4 was important for NPF events at the UB station (Deng et al., 2020b;Dada et al., 2020b). On the other hand, as shown in Fig.R3a, the H_2SO_4 concentration during 9:00- 11:00 (local time) on non-event days could be comparable with that on NPF event days, especially when CS was high. Altogether, our observation shows that the occurrence of NPF events was controlled by both H_2SO_4 and CS at the UB station (Cai et al., 2020).

3.4 Ending diameters of newly-formed grown particles

Earlier observations have shown that diameters of newly-formed particles should be larger than 70 nm to contribute to cloud condensation nuclei significantly (Man et al., 2015;Ma et al., 2021) and will be considered as haze particles when their size reaches larger than 100 nm (Kulmala et al., 2021). In Fig. R4, we show ending diameters (End Dp) of newly formed grown particles during our observations at both sites. End Dp during the observation from June 14 to July 14 at UB site (21-105 nm, with a median of 49 nm, Fig.R4a) had similar characteristics as those during the long-term observation in summer (21-126 nm, with a median of 56 nm, Fig.R4a) where most of End Dp were in the range of 25-70 nm. As shown in Fig.R4b, 61% of End Dp were in the range of 25-70 nm, and only 9% of End Dp were larger than 100 nm during our observation in summer 2018 and 2019 at UB site. We found that the ending diameters slightly higher at UB site than MT site, but the difference is not significant (49 nm vs 45 nm) as shown in Fig. R4c.

Earlier research has pointed out that in order to observe particle growth until 100 nm at a measurement station under typical conditions, simultaneous NPF should happen over a very large area (e.g. with wind speed 5 m/s and growth rate of 3 nm/h from the station to roughly 600 km upwind from the station) (Paasonen et al., 2018). During our observation in summer 2018 and 2019, most of the newly formed modes kept growing for about 20 hours after an NPF event started, and the maximum horizontal extension of the observed NPF events in the growth stage is restricted to within about 200 km (~2° in latitude) north of UB site (Fig. R5). As shown in Fig. R5, the population density is also higher within the area extending ~200 km north than beyond this limit. Therefore, it seems that NPF events were limited to the regions

with some contribution from anthropogenic emissions during air mass transport from north to Beijing. Roughly similar extent of the NPF area is also seen in other directions. However, towards the south it is more likely that increasing condensation sink from accumulating pollution becomes the limiting factor for NPF occurrence rather than decreasing strength in emission sources. NPF events at MT station had similar characteristics as those at UB station with the NPF event region extending a few hundred kilometers towards the north. The NPF events in this direction were disrupted after a relatively similar distance (or they enter the growth stagnation phase, which will be discussed in section 3.6.3). The limited NPF event area could possibly explain why most End Dp we observed were smaller than 70 nm.

3.6.3 Growth stagnation and decreasing mode diameter case during our observations

During our observations in summer 2018 and 2019 at urban site and the observation from June 14 to July 14, 2019 at MT site, there were some cases where the newly-formed particles entered a phase of growth stagnation or even displayed a decreasing mode diameter. On June 30, 2019 such case occurred simultaneously at both sites and we chose this day for a case study.

As shown in Fig.R6 a&b, the newly-formed particles entered a phase of growth stagnation almost at the same time around 12:00 at both sites. Particle mode diameters decreased from 31 nm to 15 nm at UB station around 15:00, under relatively calm meteorological condition indicating meteorological conditions could not be the reason for particles sizes decrease on June 30, 2019 at UB site. Around the same time, mode diameter at MT station also decreased gradually from 25 nm to 16 nm. Earlier observations in summer-time Beijing have speculated mode diameter decrease to be related to particle evaporation, which is triggered by favorable meteorological conditions and vapor dilution (Zhang et al., 2016). From Fig. R6, we see, that the air masses observed during the growth stagnation or diameter decrease (both marked under growth stagnation in the figure) were often located quite far in the north over the less populated areas during the onset time of regional NPF. It is also possible, that the less favorable initial conditions for particle formation and growth over these areas, combined with increasing wind speed or temporal changes in the growth rate, could explain the observations of decreasing particle sizes without evaporation (Kivekäs et al., 2016; Hakala et al., 2019).

3.5 Effect of topography

In Figure R7 we show average particle number size distribution and particle number concentration on NPF event and non-event days during our short-term parallel observation at both sites. On NPF event days, nucleation and Aitken mode particle number concentrations were much smaller at MT station than those at UB station due to smaller particle formation rates and less anthropogenic emissions. Interestingly, accumulation mode particle number concentrations were higher at MT station (701-2900 cm^{-3}, with a median of 1500 cm^{-3}) than that at UB station (350-1416 cm^{-3} with a median of 700 cm^{-3}) (Fig. R7b). Due to the close proximity of the two measurement sites, the air mass arrival directions and source regions were (mostly) similar at both sites throughout the measurement period, hence the regional and transported cannot explain the higher accumulation mode particle number concentration at MT site. As there were few primary emissions at MT site, the accumulation mode particles could be attributed to secondary particles (Kulmala et al., 2021), indicating particles at MT station were more aged than those at UB station (Fig.R7a). The possible reason is that mountains block pollution diffusion, which in the end resulted in comparable CS at MT station as UB station.

Figure R8 shows an example of the wind distribution before and during NPF event on June 30, 2019 at 850 hPa (close to the altitude of MT station) and 10 m above ground level. As shown in Fig.R8, the reanalyzed wind directions at 850 hPa were similar as those at 10 m above the ground level at MT station. Actually, the wind conditions on other NPF event days at MT station during our observation had similar characteristics tha the wind directions were similar between 850 hPa and 10 m above ground level indicating air masses well mixed during NPF event. Earlier observations also found NPF event happened uniformly within the mixing layer at their observation stations and particle number size distribution remains roughly constant within the mixing layer (Shen et al., 2018; Lampilahti et al., 2021).

Figures

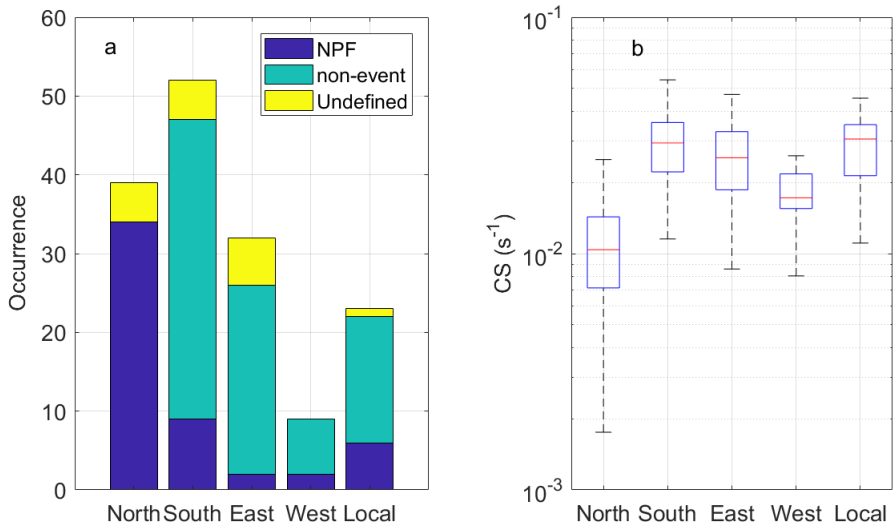

Figure R1: Occurrence of NPF events and non-events under air masses arriving from different directions (a) as well as medians and percentiles of condensation sink (CS, s^{-1}) during the 9:00-11:00 (local time) under different air masses (b) during our observation in summer 2018 and 2019 at UB station. The red line represents the median of the data and the lower and upper edges of the box represent 25th and 75th percentiles of the data, respectively. The length of the whiskers represents 1.5× interquartile range which includes 99.3% of the data. Data outside the whiskers are considered outliers and are marked with red crosses. The time resolution of CS was 8 min.

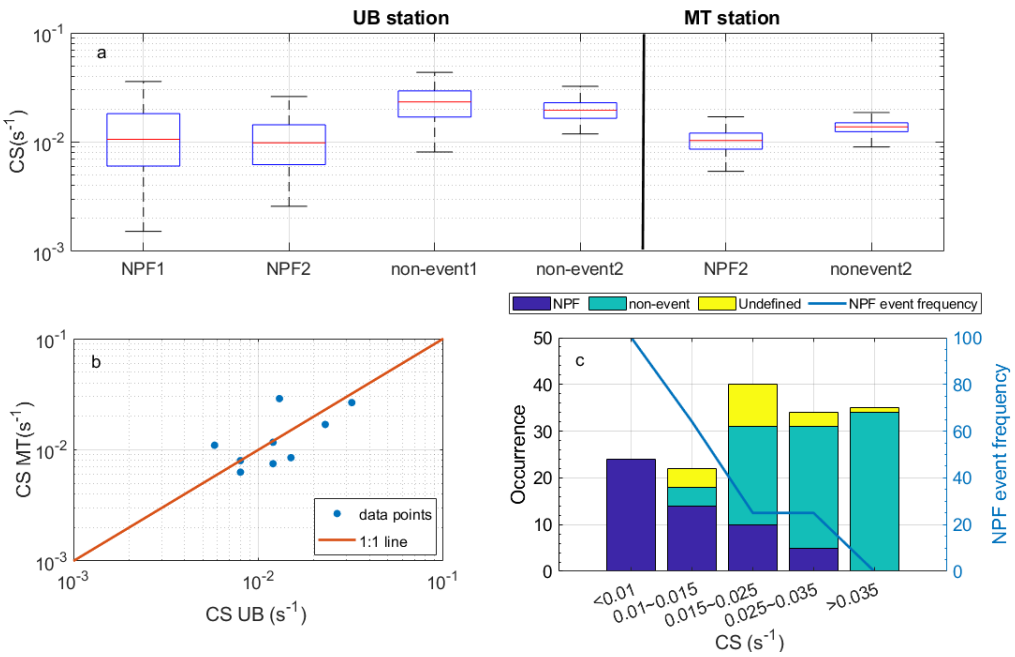

Figure R2: (a) Median and percentiles of condensation sink (CS, s^{-1}) during our observations at both stations. The 'NPF1' and 'non-event1' referred to NPF and non-event days during summer 2018 and 2019, while 'NPF2' and 'non-event2' referred to NPF and non-event days during the short-term parallel observation from June 14 to July 14, 2019 at both sites. The red line represents the median of the data and the lower and upper edges of the box represent 25th and 75th percentiles of the data, respectively. The length of the whiskers represents 1.5× interquartile range which includes 99.3% of the data. The time resolution of CS was 8 min. (b) Median CS during the first 2 hours of NPF events on common NPF event days measured at both stations. (c) Numbers of NPF event, non-event and undefined days as well as NPF event frequency as a function of CS during our observation in summer 2018 and 2019 at UB station.

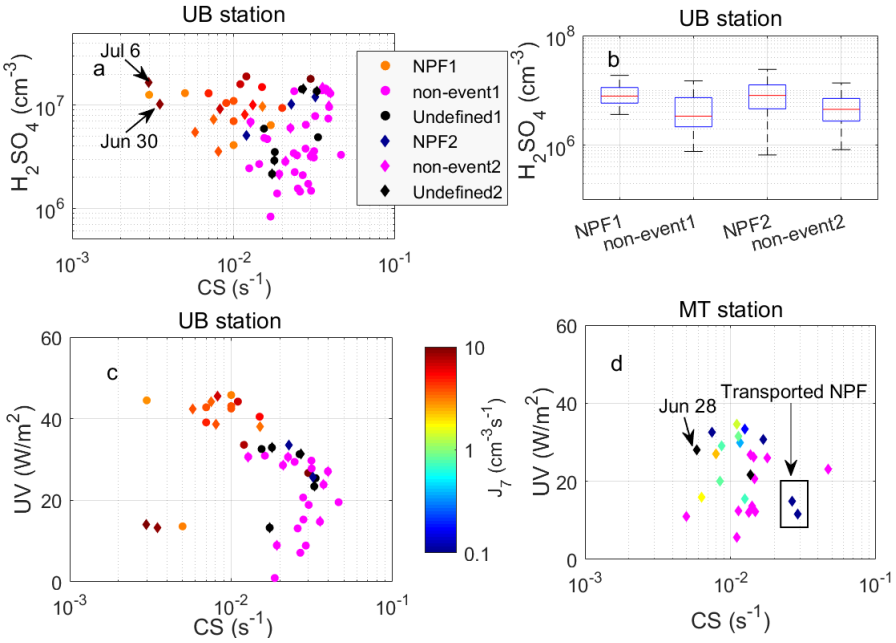

Figure R3: (a) Median condensation sinks (CS, s^{-1}) and H_2SO_4 concentration (SA, cm^{-3}) and (b) solar radiation (UVA+UVB, W/m^2) during the first 2 hours of every NPF event and 9:00-11:00 on every non-event day at UB station. (c) median and percentiles of H_2SO_4 concentration observed at UB station during the first 2 hours of NPF events and 9:00-11:00 on non-event days. The 'NPF1' and 'non-event1' referred to NPF event and non-event days in summer 2018 and 2019 and the 'NPF2' and 'non-event2' referred to NPF event and non-event days during the observation from June 14 to July 14, 2019. (d) Median condensation sinks (CS, s^{-1}) and solar radiation (UVA+UVB, W/m^2) during the first 2 hours of every NPF event and 9:00-11:00 on every non-event day at MT station. Transported NPF event cases and one non-event day with air masses belonging to west group (Jun 28) were all pointed out in the figure. Color of data points on NPF event days means particle formation rate (J_7, $cm^{-3}s^{-1}$) when it can be calculated reliably. The time resolution of CS was 8 min at UB station and 4 min at MT station, respectively. The time resolution was 30 min for SA data at UB station and 1h for solar radiation data at both stations.

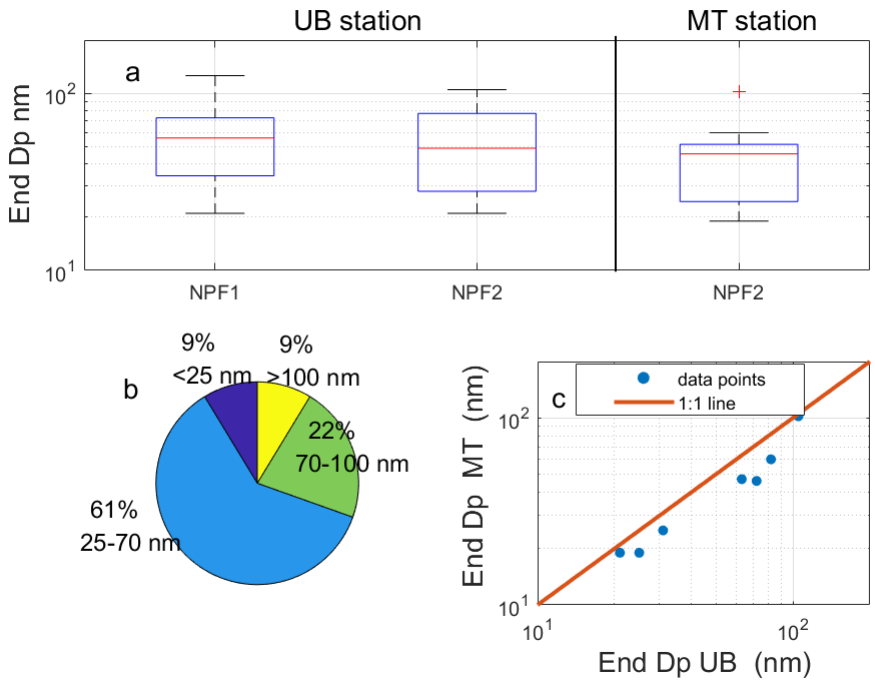

Figure R4: (a) Median and percentiles of end diameters (D_{pend}, nm) of NPF events measured at both sites. The red line represents the median of the data and the lower and upper edges of the box represent 25th and 75th percentiles of the data, respectively. The length of the whiskers represents 1.5× interquartile range which includes 99.3% of the data. The 'NPF1' and 'non-event1' referred to NPF event and non-event days in summer 2018 and 2019 and the 'NPF2' and 'non-event2' referred to NPF event and non-event days during the observation from June 14 to July 14, 2019. (b) Frequencies of end diameters in the size range of smaller than 25 nm, 25-70 nm, 70-100 nm and above 100 nm during our observation at UB station in summer 2018 and 2019. (c) Comparison between end diameters of common NPF events at both stations.

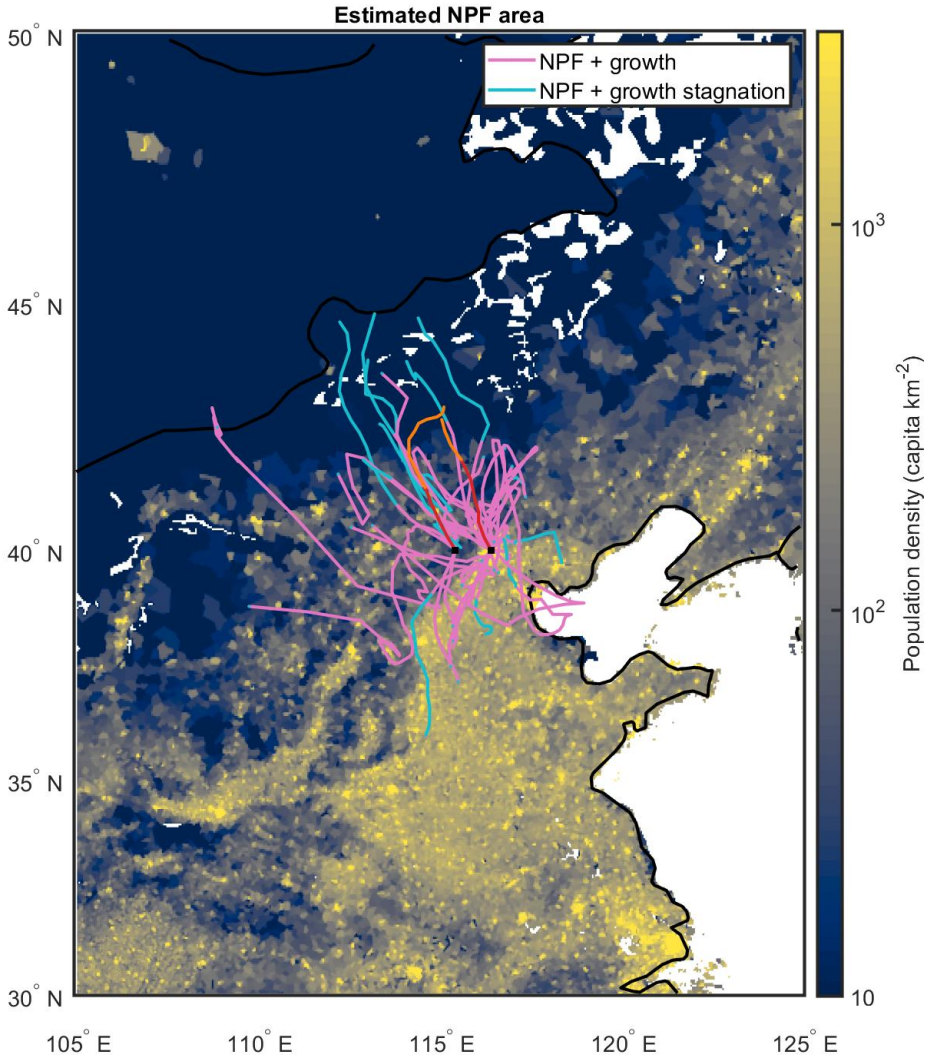

Figure R5: Spatial extent of the area where new particle formation events are estimated to have taken place based on air mass back trajectories and the observed NPF events at both sites. Each line represents a single NPF event and extends to the point beyond which continuation of the mode formed in an NPF event was no longer observed at the measurement site. In other words, if an air mass is located outside the area roughly outlined by the colored lines during the typical onset time of NPF and then transported to our measurement sites, NPF is unlikely to have occurred in said air mass. The lines change color from pink to light blue if the observed NPF event enters a stage of growth stagnation, which can indicate a less favorable environment for the formation and growth of new particles. The lines for the case study day of June 30, 2019 are marked with red and change color to orange

if growth stagnation occurs. The lines are overlaid on top of a population density map (Gridded Population of the World; GPWv4.10; CC BY 4.0), which is used to illustrate the level of anthropogenic activities and emissions.

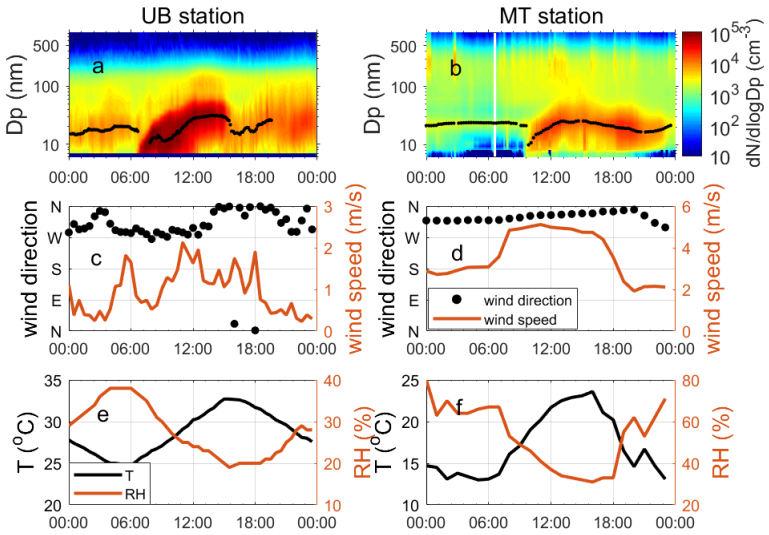

Figure R6: Time series of particle number size distribution and mode diameters (a, b), wind speed and direction (c, d), temperature and RH (e, f) measured at UB (left panel) and MT (right panel) on June 30, 2019.

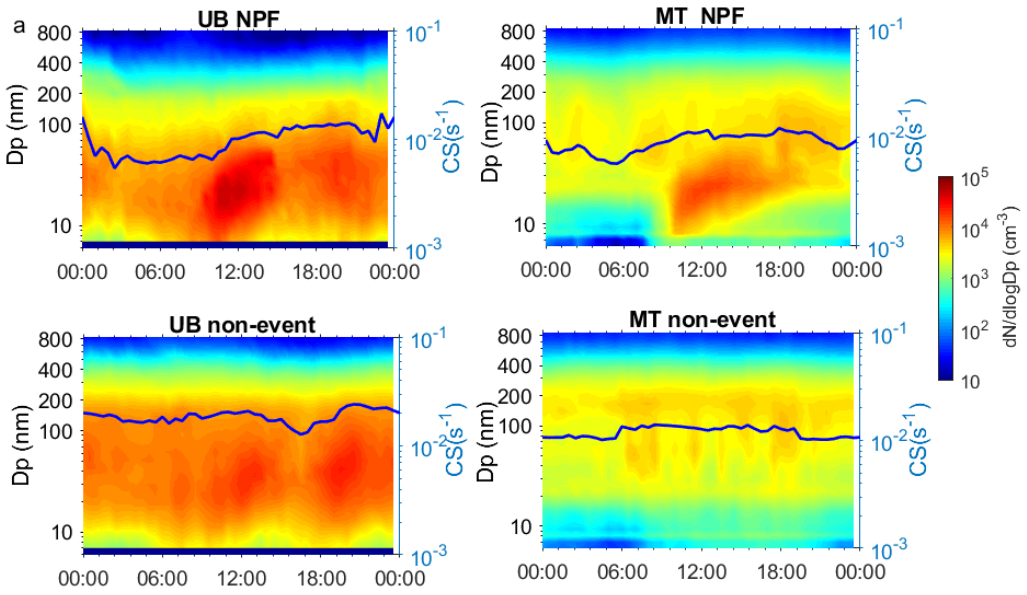

Figure R7: (a) Median particle number size distribution as well as CS (blue lines) on NPF event and non-event days at UB (left panel) and MT (right panel) stations and (b) median and percentiles of nucleation, Aitken and accumulation modes particle number concentration on NPF event and non-event days during our observation from June 14 to July 14, 2019 at both stations. The red line represents the median of the data and the lower and upper edges of the box represent 25th and 75th percentiles of the data, respectively. The length of the whiskers represents 1.5× interquartile range which includes 99.3% of the data. Data outside the whiskers are considered outliers and are marked with red crosses.

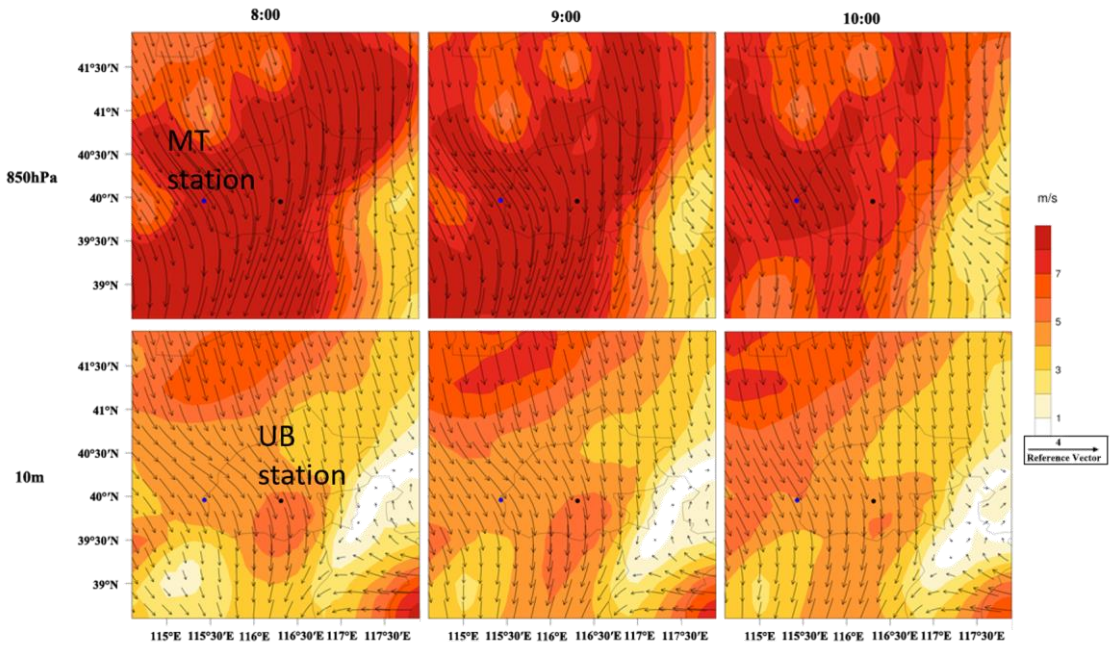

Figure R8: Wind distribution at 8:00, 9:00 and 10:00 on June 30, 2019 at 10 m above the ground level and 850 hPa (close to the altitude of MT station). The blue and black points on the figures represent MT and UB stations, respectively.

References

Cai, R., Yang, D., Fu, Y., Wang, X., Li, X., Ma, Y., Hao, J., Zheng, J., and Jiang, J.: Aerosol surface area concentration: a governing factor in new particle formation in Beijing, Atmos Chem Phys, 17, 12327-12340, 10.5194/acp-17-12327-2017, 2017.

Deng, C., Cai, R., Yan, C., Zheng, J., and Jiang, J.: Formation and growth of sub-3 nm particles in megacities: impact of background aerosols, Faraday Discuss, 10.1039/d0fd00083c, 2020a.

Deng, C., Fu, Y., Dada, L., Yan, C., Cai, R., Yang, D., Zhou, Y., Yin, R., Lu, Y., Li, X., Qiao, X., Fan, X., Nie, W., Kontkanen, J., Kangasluoma, J., Chu, B., Ding, A., Kerminen, V. M., Paasonen, P., Worsnop, D. R., Bianchi, F., Liu, Y., Zheng, J., Wang, L., Kulmala, M., and Jiang, J.: Seasonal Characteristics of New Particle Formation and Growth in Urban Beijing, Environ Sci Technol, 54, 8547-8557, 10.1021/acs.est.0c00808, 2020b.

Hakala, S., Alghamdi, M. A., Paasonen, P., Vakkari, V., Khoder, M. I., Neitola, K., Dada, L., Abdelmaksoud, A. S., Al-Jeelani, H., Shabbaj, I. I., Almehmadi, F. M., Sundström, A.-M., Lihavainen, H., Kerminen, V.-M., Kontkanen, J., Kulmala, M., Hussein, T., and Hyvärinen, A.-P.: New particle formation, growth and apparent shrinkage at a rural background site in western Saudi Arabia, Atmos Chem Phys, 19, 19, https://doi.org/10.5194/acp-19-10537-2019, 2019.

Kivekäs, N., Carpman, J., Roldin, P., Leppä, J., O'Connor, E., Kristensson, A., and Asmi, E.: Coupling an aerosol box model with one-dimensional flow: a tool for understanding observations of new particle formation events, Tellus B, 68, 29706, doi:10.3402/tellusb.v68.29706, 2016.

Kristensson, A., Johansson, M., Swietlicki, E., Kivekäs, N., Hussein, T., Nieminen, T., Kulmala, M., and Dal Maso, M.: NanoMap: geographical mapping of atmospheric new particle formation through analysis of particle number size distribution data, Boreal Environ. Res., 19 (suppl. B), 329—342, 2014.

Kulmala, M., Kerminen, V. M., Petäjä, T., Ding, A. J., Wang, L.: Atmospheric gas-to-particle conversion: why NPF events are observed in megacities?, Faraday Discuss, 271-288,

https://doi.org/10.1039/C6FD00257A, 2017.

Kulmala, M., Dada, L., Dällenbach, K., Yan, C., Stolzenburg, D., Kontkanen, J., Ezhova, E., Hakala, S., Tuovinen, S., Kokkonen, T., Kurppa, M., Cai, R., Zhou, Y., Yin, R., Baalbaki, R., Chan, T., Chu, B., Deng, C., Fu, Y., Ge, M., He, H., Heikkinen, L., Junninen, H., Nei, W., Rusanen, A., Vakkari, V., Wang, Y., Wang, L., yao, l., Zheng, J., Kujansuu, J., Kangasluoma, J., Petäjä, T., Paasonen, P., Järvi, L., Worsnop, D., Ding, A., Liu, Y., Jiang, J., Bianchi, F., Yang, G., Liu, Y., Lu, Y., and Kerminen, V.-M.: Is reducing new particle formation a plausible solution to mitigate particulate air pollution in Beijing and other Chinese megacities?, Faraday Discuss, 10.1039/d0fd00078g, 2021.

Liu, J. Q., Jiang, J. K., Zhang, Q., Deng, J. G., and Hao, J. M.: A spectrometer for measuring particle size distributions in the range of 3 nm to 10 mu m, Front Env Sci Eng, 10, 63-72, https://doi.org/10.1007/s11783-014-0754-x, 2016.

Wang, Z. B., Hu, M., Sun, J. Y., Wu, Z. J., Yue, D. L., Shen, X. J., Zhang, Y. M., Pei, X. Y., Cheng, Y. F., and Wiedensohler, A.: Characteristics of regional new particle formation in urban and regional background environments in the North China Plain, Atmos Chem Phys, 13, 12495-12506, 10.5194/acp-13-12495-2013, 2013.

Ma, L., Zhu, Y., Zheng, M., Sun, Y., Huang, L., Liu, X., Gao, Y., Shen, Y., Gao, H., and Yao, X.: Investigating three patterns of new particles growing to the size of cloud condensation nuclei in Beijing's urban atmosphere, Atmos Chem Phys, 21, 183-200, 10.5194/acp-21-183-2021, 2021.

Man, H. Y., Zhu, Y. J., Ji, F., Yao, X. H., Lau, N. T., Li, Y. J., Lee, B. P., and Chan, C. K.: Comparison of Daytime and Nighttime New Particle Growth at the HKUST Supersite in Hong Kong, Environ Sci Technol, 49, 7170-7178, 2015.

Shen, X., Sun, J., Kivekäs, N., Kristensson, A., Zhang, X., Zhang, Y., Zhang, L., Fan, R., Qi, X., Ma, Q., and Zhou, H.: Spatial distribution and occurrence probability of regional new particle formation events in eastern China, Atmos Chem Phys, 18, 587-599, 10.5194/acp-18-587-2018, 2018.

Lampilahti, J., Manninen, H. E., Nieminen, T., Mirme, S., Ehn, M., Pullinen, I., Leino, K., Schobesberger, S., Kangasluoma, J., Kontkanen, J., Järvinen, E., Väänänen, R., Yli-Juuti, T., Krejci, R., Lehtipalo, K., Levula, J., Mirme, A., Decesari, S., Tillmann, R., Worsnop, D. R.,

Rohrer, F., Kiendler-Scharr, A., Petäjä, T., Kerminen, V.-M., Mentel, T. F., and Kulmala, M.: Zeppelin-led study on the onset of new particle formation in the planetary boundary layer, Atmospheric Chemistry and Physics Discussions, 10.5194/acp-2021-282, 2021.

Paasonen, P., Peltola, M., Kontkanen, J., Junninen, H., Kerminen, V.-M., and Kulmala, M.: Comprehensive analysis of particle growth rates from nucleation mode to cloud condensation nuclei in boreal forest, Atmos Chem Phys, 18, 12085-12103, 10.5194/acp-18-12085-2018, 2018.

Zhang, J., Chen, Z., Lu, Y., Gui, H., Liu, J., Wang, J., Yu, T., and Cheng, Y.: Observations of New Particle Formation, Subsequent Growth and Shrinkage during Summertime in Beijing, Aerosol Air Qual Res, 16, 1591-1602, 10.4209/aaqr.2015.07.0480, 2016.